Journal of Nuclear Materials 487 (2017) 186–191

Contents lists available at ScienceDirect

Journal of Nuclear Materials

journal homepage: www.elsevier.com/locate/jnucmat

Phase diagram of the Fe-Sn-Zr system at 800 °C

N. Nieva [a], C. Corvalán [b, *], M.J. Jiménez [c], A. Gómez [d], C. Arreguez [a], J.-M. Joubert [e], D. Arias [f]

[a] Laboratorio de Física del Sólido, Departamento de Física, Facultad de Ciencias Exactas y Tecnología, Universidad Nacional de Tucumán, Argentina
[b] Gerencia de Materiales, Comisión Nacional de Energía Atómica Argentina (CNEA), Universidad Nacional de Tres de Febrero, Argentina, CONICET, Consejo Nacional de Ciencia y Técnica, Argentina
[c] IFISUR, CONICET, Departamento de Física, Universidad Nacional del Sur, Bahía Blanca, Argentina
[d] Grupo LMFAE – PPFAE, Centro Atómico Ezeiza, Comisión Nacional de Energía Atómica, Argentina
[e] Chimie Métallurgique des Terres Rares (CMTR), Institut de Chimie et des Matériaux Paris-Est (ICMPE), CNRS, Université Paris-Est Créteil, 2-8 rue Henri Dunant, 94320 Thiais Cedex, France
[f] Instituto de Tecnología J. Sabato, Universidad Nacional de San Martín-CNEA, Argentina

HIGHLIGHTS

- A phase diagram of Fe-Sn-Zr system at 800 °C is proposed.
- The isothermal section of Fe-Sn-Zr system at 800 °C and that at 900 °C determined previously allow reliable extrapolations at low temperatures.
- The study at different temperatures (900 °C and 800 °C in this case) is highly desirable because it allows the separation between enthalpic and entropic effects in a future Calphad modelling.

ARTICLE INFO

Article history:
Received 3 November 2016
Received in revised form
23 December 2016
Accepted 25 January 2017
Available online 1 February 2017

Keywords:
Phase diagrams
Zirconium
Fe-Sn-Zr system

ABSTRACT

New experimental results on the Fe-Sn-Zr phase diagram at 800 °C are presented, particularly in the central, Fe rich and Sn rich regions of the Gibbs triangle. Seven ternary alloys were designed, produced and examined by different techniques: optical and scanning electron microscopy, semi-quantitative microanalysis, quantitative microanalysis and X-ray diffraction. The results of this work and previous experimental data were used to determine the phase diagram section at 800 °C which contains at least five ternary compounds: Fe_6Sn_6Zr, Y, X′, θ and *C*36.

1. Introduction

Metal alloys based on Zr are widely used in the nuclear industry and technology. They are mainly used as cladding and structure materials in light and heavy water nuclear reactors. This is due to their specific characteristics: good corrosion resistance, good mechanical properties, high resistance to radiation damage and low cross section of capture for thermal neutrons. Security is essential for materials with nuclear functions. An important way to achieve this issue is to have a complete understanding of the physical metallurgy of materials and the thermo-mechanical processes involved in the final elaboration of technological products. In this way, for a correct, safe and efficient use of the products the knowledge of phase diagrams is very important.

The phase diagram of the ternary Fe-Sn-Zr system was investigated mainly by Tanner and Levinson [1], Kudryatsev and Tregubov [2], Korotkova [3], Nieva and Arias [4–6] and Savidan et *al.* [7]. The phase relations in the Zr rich corner up to cubic Fe_2Zr and $SnZr_4$ have been investigated by Tanner and Levinson [1] using X-ray diffraction (XRD) and metallography in the temperature range between 700 and 1100 °C. Tanner found a ternary phase θ with the composition range of Zr (matrix)-Fe (11.6–13.1) at% - Sn 19.1 at%. The crystal structure of this phase was first determined by Kwon et *al.* [8], with a narrow homogeneity range according to Tanner. Kwon reported that it had the Al_2CoZr_6 hexagonal structure type compound. Kudryatsev and Tregubov [2] analyzed the Zr rich

* Corresponding author.
E-mail address: corvalan@cnea.gov.ar (C. Corvalán).

http://dx.doi.org/10.1016/j.jnucmat.2017.01.050
0022-3115/

region of the Fe-Sn-Zr system by means of microstructure studies and measurements of hardness and microhardness, but did not report the presence of the θ phase. Through XRD, electron microscopy and electron-probe microanalysis (EPMA), Korotkova [3] outlined a phase diagram for the ternary system in the region of Zr-Fe_2Zr-Sn_3Zr_5 and the temperature range from 500 to 1600 °C. This work confirmed the existence of the ternary compound θ reported by Ref. [1]. Subsequently, a critical review for the Fe-Sn-Zr system was performed by Raghavan [9] who mainly evaluated the results of Refs. [1–3] and presented two 'tentative' isothermal sections (700 and 1100 °C).

Nieva and Arias [4,5] analyzed the region of the phase diagram located near the composition of a master alloy of Zircaloy-4 [10], and found two new ternary compounds (N phase and X phase) in the central region of the Fe-Sn-Zr Gibbs triangle. Afterwards, the same authors investigated the reported phases and their equilibrium relationships in an extended area of the Gibbs triangle, at 800 and 900 °C, by means of different complementary techniques: quantitative analysis with EPMA, qualitative analysis with electron scanning microscopy and X-ray energy dispersive spectrometry (SEM-EDS), XRD and metallographic examination [6]. In this work, Nieva and Arias confirmed the existence of the formerly reported θ, N and X phases, and suggested that the θ and X phases have extended single phase regions. Also, they observed that, at both temperatures: 1) $SnZr_4$ and Sn_3Zr_5 showed a low solubility of Fe, 2) Fe had an important solubility in the Sn_4Zr_5 phase and 3) $FeZr_2$ and $FeZr_3$ phases show low solubility of Sn. An important solubility of Sn in Fe_2Zr was measured (up to 10 at%, at 800 °C) and a 'sluggish' behavior in the nucleation and growth processes of $SnZr_4$ was also verified by Nieva and Arias in this work.

Literature data of the ternary system phase diagrams up to 2009 were reviewed by Liu et *al.* [11], mainly focusing on those diagrams proposed by Raghavan [9] at 700 and 1100 °C in Zr-Fe_2Zr-Sn_3Zr_5 region and the most widespread 800 and 900 °C diagrams proposed by Nieva and Arias [6]. Savidan et *al.* [7] completed the phase diagram of this system at 900 °C, starting from the work of Nieva and Arias [6] and adding own experimental results. Savidan et *al.* characterized the samples employing XRD, optical metallography, scanning electron microscopy (SEM) and EPMA techniques and methods. They confirmed the existence of the ternary N phase, determining that it has an orthorhombic crystal structure with $Ga_6Mn_2Sc_3$ type and lattice parameters: a = 8.175 Å, b = 8.930 Å, c = 10.720 Å. They also showed that the X phase homogeneity domain consisted in fact of two separate compounds with close compositions (X′ and X″). The crystal structures of these compounds are still unresolved. They also reported the existence of three other ternary compounds: Fe_6Sn_6Zr phase, Y and *C*36. The first one crystallizes in the Fe_6Ge_6Mg (also called Fe_6Ge_6Hf) structure type. This structure derives from the CoSn structure type of the FeSn compound, by ordering of interstitial Zr atoms in half of the Sn8 bipyramidal sites yielding a doubling of the c parameter [12]. The crystal structure of Y is still unknown. The mentioned *C*36 compound has been identified as a Laves phase with $MgNi_2$ type hexagonal crystal structure. It derives from the binary hexagonal *C*36 reported in the Fe-Zr system, as existing between 1240 °C and 1345 °C and formed by the peritectic reaction $Fe_2Zr(C15) + L \leftrightarrow C36$ [13]. Nieva et *al.* [14] also reported that in the same region, analyzing Fe-Sn-Zr at 1100 °C, the *C*36 phase is stabilized by the addition of Sn. Something similar was observed in the Fe-Sb-Zr system where the addition of Sb generates a *C*36 hexagonal phase at 800 °C, called Zr $(Fe_{1-x}Sb_x)_{2-y}$ by the authors [15].

To summarize, a complete isothermal section at 900 °C and a partial isothermal section at 800 °C are available for the Fe-Sn-Zr system. The purpose of this work was to complete the 800 °C section for the three following reasons:

- the temperature is more closer to the actual temperature in nuclear power plants (350 °C in pressurized water reactors) so this section may better represent the behavior of the alloys in the frame of their application. A study at even lower temperature would be welcome but the annealing time to reach equilibrium may become prohibitive so that we believe 800 °C is the lowest accessible temperature for equilibrium measurements. Additionally, the materials characterization at different temperatures is important for nuclear reactor accidents, like LOCA (Loss Of Coolant Accident) with a temperature range of 800 °C–1200 °C.
- the study at a temperature different from 900 °C is highly desirable because it allows the separation between enthalpic and entropic effects in a future Calphad modelling of this system if different stable phases are found or if we can locate invariant reactions. Higher temperature than 900 °C are difficult to study because of the growing importance of the liquid phase in the binary system Fe-Sn and Sn-Zr, so 800 °C was chosen.
- we have a special interest in the stability of the *C*36 phase present at 900 °C and the relative stability with the $Fe_2Zr(C15)$ phase. It has been described by Savidan et *al.* [7] as an extension in the ternary field to low temperatures of the binary *C*36 phase in the Fe-Zr system [13] in which it exists only above 1240 °C. If this is the case, then its homogeneity domain should shrink and the phase is expected to disappear when the temperature gets lower.

2. Experimental

Seven ternary alloys were designed to analyze the area of interest. They were labeled as A1 to A7, synthesized and submitted to heat treatments. The present phases were identified using metallographic techniques (optical microscope Olympus BX-60M), X-ray diffraction (XRD, BRUKER AXS D8 diffractometer), scanning electron microscopy analysis with energy dispersive spectrometry (SEM-EDS, JEOL, Thermo and FEI INSPECT S50) and quantitative microanalysis using electron microprobe with wavelength dispersive spectrometry (SEM-WDS microprobe JEOL JXA-8230).

2.1. Synthesis of the alloys

The raw materials were zirconium (99.95 wt%), tin (99.999 wt%) and iron (99.95 wt%). Buttons (~10 g) were prepared in an arc furnace with a non-consumable tungsten electrode and a water-cooled copper crucible, in a high purity argon atmosphere (99.999%). The alloys were melted at least four times and turned upside down between each melting. Not significant weight losses were registered.

2.2. Heat treatments

The alloys A1, A4, A5, A6 and A7 were heat treated (HT) at 800 °C-20578 h. For higher Sn content (alloys A2 and A3), the heat treatment was 800 °C–3058 h. The samples were carefully cleaned, wrapped in tantalum sheets and placed in a silica glass tube previously cleaned and dried. The tube was purged with high purity Ar gas and sealed maintaining internal pressure of Ar. At the end of the heat treatment the samples were quenched in water without breaking the seal.

2.3. Sample preparation

After the heat treatments the samples were prepared for characterization. For the quantitative microanalysis, samples were ground with Si carbide paper and polished with cloth and diamond paste down to a particle size of 0.25 μm. For metallographic inspection (with light and electron microscopy) and SEM-EDS

analysis, after the steps of grinding and polishing, the samples were chemically etched. The samples with higher contents of Zr were etched with an aqueous solution of nitric and hydrofluoric acid. Those alloys with higher Fe content were etched with diluted nitric acid. X-ray analyzes were made on polished samples radiating over an area of approximately 15 mm × 15 mm.

3. Results

Table 1 shows the nominal composition of alloys labeled as A1 to A7. Also, it shows the identified phases with crystal structure and chemical compositions of the samples HT at 800 °C. Crystal structure was obtained from the results of X-ray and chemical compositions from WDS and EDS measurements. The low quantity of phases, the peak overlays of different phases and the no determination of some crystal structure, make the profile refinement with particular difficulties and some lattice parameters were not found.

In the central area of the diagram, where alloy A1 is placed, at 800 °C three phases were observed: two ternary phases, the N phase and the X′ phase, and one binary phase, the Fe_2Zr (*C*15) phase. Although the crystal structure of the X′ phase is unknown, the diffraction peaks generated by this crystalline phase are known [7] and there were used to identify the presence of this phase in this sample. The binary phase Fe_2Zr (*C*15), with $MgCu_2$ type cubic structure, has an important Sn solubility. As above mentioned, this same feature was observed by Nieva and Arias [6] in this system but on other alloy $Zr_{40}Fe_{40}Sn_{20}$ at% at 800 °C. Fig. 1 shows a typical microstructure of this sample.

The alloy A2 (the one with the highest content of Sn) HT at 800 °C showed the presence of three phases: the Sn phase with little Fe and Zr in solution (liquid phase at 800 °C), the N phase and the Fe_6Sn_6Zr phase.

The alloy A3 HT at 800 °C presented a field of three phases: the N phase, the Fe_6Sn_6Zr phase and the Y phase. As for the X′ phase, the diffraction peaks of Y crystalline phase are also known from the work of Savidan et *al.* [7].

The alloy A4 HT at 800 °C is in a two-phase field, the N phase and the cubic Fe_2Zr(*C*15) phase. The micrograph of Fig. 2 shows the microstructure of the two identified phases in this sample. Also, as an example, the diffraction pattern and the Rietveld refinement is shown in Fig. 3.

The alloy A5 HT at 800 °C showed the existence of three main phases: the Fe(α) phase, the ternary Y phase and the hexagonal ternary phase *C*36. Fig. 4 shows the typical microstructure of this sample.

The alloy A6 HT at 800 °C presented a two-phase field: the Fe(α) cubic phase and the hexagonal *C*36 phase. On the other hand, the A7 alloy, HT at 800 °C, is in another two-phase field: the Fe(α) phase and the cubic Fe_2Zr(*C*15) phase. The micrographs of Figs. 5 and 6 show the typical microstructure of both samples.

4. Discussion

Based on the results of the present work, the study of the Zr-rich corner of Nieva and Arias [6] and the reports of Savidan et *al.* [7], a ternary section of the Fe-Sn-Zr system at 800 °C is presented in Fig. 7.

A total of seven ternary phases are proposed at this temperature. The existence of at least five new ternary compounds in the studied region at this temperature is reported in the present work: X′, X″ (added considering the reports at 900 °C [7]), Y, Fe_6Sn_6Zr and *C*36 phases. The two remaining ternary phases are the previously reported N (also observed in this work) and θ phases.

Four compatibility triangles are resolved: [Fe(α)-Y-*C*36], [Y-Fe_6Sn_6Zr-N], [Fe_6Sn_6Zr-Sn(liq)-N] and [Fe_2Zr(*C*15)-N-X′]. The two-phase [Fe(α)-*C*36], [Fe(α)-Fe_2Zr(*C*15)] and [Fe_2Zr(*C*15)-N]regions

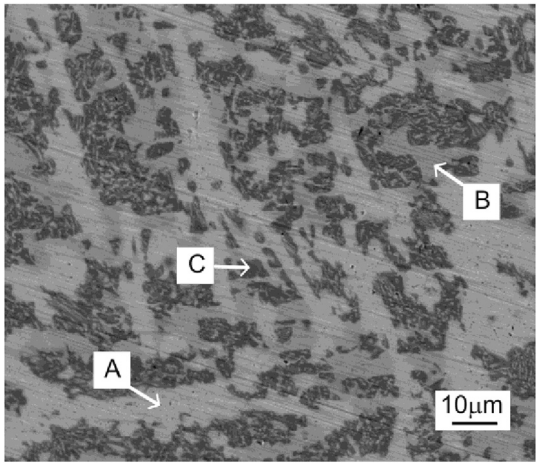

Fig. 1. Back scattered electron SEM image of A1 sample, heat treatment at 800 °C. Identified phases: A: Fe_2Zr(*C*15) (light grey); B: X′ (grey); C:N (dark grey).

Table 1
Nominal compositions of the alloys, heat treatment duration, characterization of the samples: phase identification (XRD), chemical compositions (EPMA), structure type and lattice parameters (from XRD) in the 800 °C HT samples. When possible to calculate, the standard deviation of compositions was less than 0.3 at%.

Samples	Nominal composition [at%]	HT at 800 °C [Hours]	Phases	Phase compositions [at%]	Structure type	Lattice parameters [Å]
A1	$Fe_{40}Sn_{28}Zr_{32}$	20578	*C*15	$Fe_{65.3}$ $Sn_{10.1}$ $Zr_{24.6}$	Cu_2Mg	a = 7.090
			N	$Fe_{36.5}$ $Sn_{36.4}$ $Zr_{27.1}$	$Ga_6Mn_2Sc_3$	a = 8.175 b = 8.936 c = 10.729
			X′	$Fe_{17.6}$ $Sn_{39.7}$ $Zr_{42.7}$	–	–
A2	$Fe_{40}Sn_{50}Zr_{10}$	3058	Sn(β)	$Fe_{3.2}$ $Sn_{93.2}$ $Zr_{3.6}$	Snβ	a = 5.832 c = 3.182
			Fe_6Sn_6Zr	$Fe_{49.8}$ $Sn_{44.3}$ $Zr_{5.9}$	Fe_6Ge_6Mg	Fe_6Sn_6Zr
			N	$Fe_{34.9}$ $Sn_{37.0}$ $Zr_{28.1}$	$Ga_6Mn_2Sc_3$	a = 8.174 b = 8.932 c = 10.719
A3	$Fe_{55}Sn_{30}Zr_{15}$	3058	Fe_6Sn_6Zr	$Fe_{47.9}$ $Sn_{44.3}$ $Zr_{7.8}$	Fe_6Ge_6Mg	–
			Y	$Fe_{55.9}$ $Sn_{29.0}$ $Zr_{15.1}$	–	–
			N	$Fe_{35.7}$ $Sn_{36.3}$ $Zr_{28.0}$	$Ga_6Mn_2Sc_3$	–
A4	$Fe_{55}Sn_{20}Zr_{25}$	20578	*C*15	$Fe_{65.4}$ $Sn_{11.9}$ $Zr_{22.7}$	Cu_2Mg	a = 7.082
			N	$Fe_{37.1}$ $Sn_{35.8}$ $Zr_{27.1}$	$Ga_6Mn_2Sc_3$	a = 8.168 b = 8.937 c = 10.739
A5	$Fe_{65}Sn_{20}Zr_{15}$	20578	*C*36	$Fe_{63.3}$ $Sn_{18.7}$ $Zr_{18.0}$	Cu_2Ni	a = 4.970 c = 16.143
			Y	$Fe_{57.1}$ $Sn_{28.1}$ $Zr_{14.8}$	–	–
			Fe (α)	$Fe_{96.5}$ $Sn_{3.2}$ $Zr_{0.3}$	W	a = 2.885
A6	$Fe_{90}Sn_5Zr_5$	20578	Fe (α)	$Fe_{97.7}$ $Sn_{2.1}$ $Zr_{0.2}$	W	a = 2.868
			*C*36	$Fe_{68.0}$ $Sn_{13.8}$ $Zr_{18.2}$	Cu_2Ni	a = 4.994 c = 16.261
A7	$Fe_{87}Sn_3Zr_{10}$	20578	Fe (α)	$Fe_{99.5}$ $Sn_{0.3}$ $Zr_{0.2}$	W	a = 2.883
			*C*15	$Fe_{68.7}$ $Sn_{7.7}$ $Zr_{23.6}$	Cu_2Mg	a = 7.030

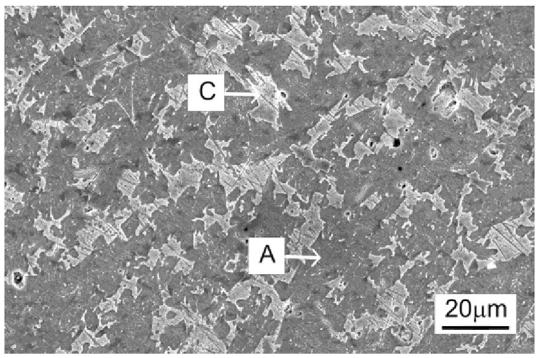

Fig. 2. Secondary electron SEM image of A4 sample, heat treatment at 800 °C. Identified phases: A: Fe_2Zr (*C*15) (dark grey); C: N (light grey).

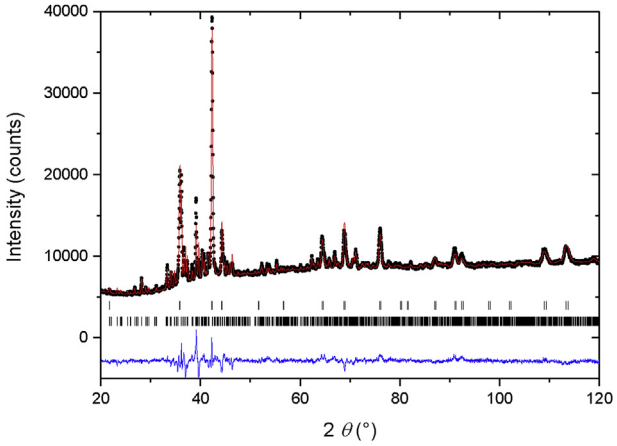

Fig. 3. Rietveld plot obtained for A4 sample HT at 800 °C. The measured and calculated diagrams are shown with the difference curve below. The vertical bars indicate the position of the reflections for the indexed phases Fe_2Zr(*C*15) and N.

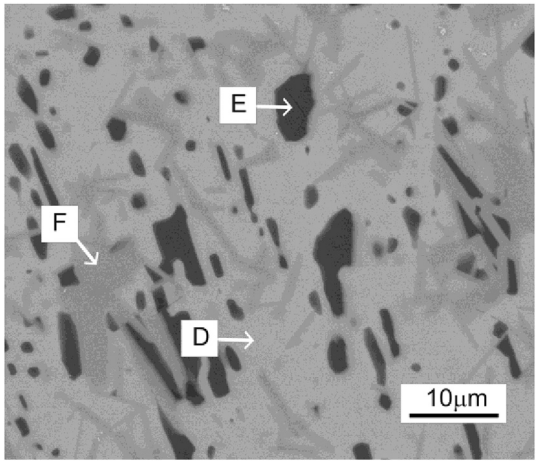

Fig. 4. Back scattered electron SEM image of A5 sample, heat treatment at 800 °C. Identified phases: D: Y (light grey); E: Fe(α) (black); F: *C*36 (dark grey).

are also resolved.

Compatibility triangles [Fe(α)-Fe_6Sn_6Zr-Y], [*C*36-Y-N], [Fe_2Zr(*C*15)-*C*36-N], [N-Sn_2Zr-X″], [X″-Sn_2Zr-Sn_4Zr_5], [N-X″ -X′] and [X′-X″-Sn_4Zr_5] are drawn taking into account the results of Savidan et *al.* [7] at 900 °C. Region between the Fe-Sn binary and Fe_6Sn_6Zr

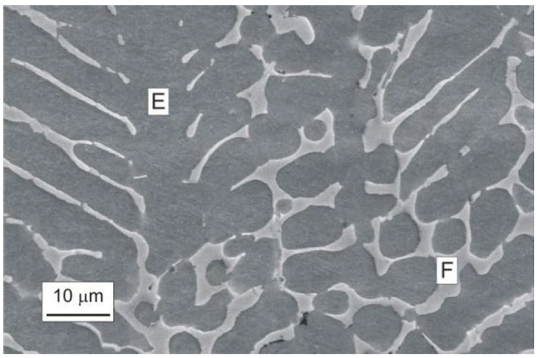

Fig. 5. Back scattered electron SEM image of A6 sample, heat treatment at 800 °C. Identified phases: E: Fe(α) (dark grey); F: *C*36 (light grey).

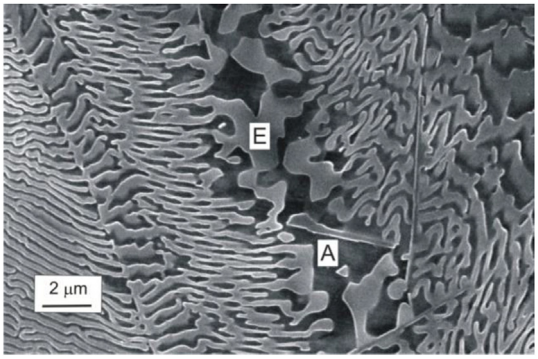

Fig. 6. Secondary electron SEM image of A7 sample, heat treatment at 800 °C. E: Fe(α) (light grey) and A (dark grey) is the normal place of Fe_2Zr(*C*15) phase.

phase is completed from the binary diagram [17]. Compatibility triangles [Fe(α)-Fe_5Sn_3-Fe_6Sn_6Zr], [Fe_5Sn_3-Fe_3Sn_2-Fe_6Sn_6Zr] and [Fe_3Sn_2-Sn(liq)-Fe_6Sn_6Zr] are proposed as probable.

Ternary region between compounds Fe_2Zr(*C*15), Sn_3Zr_5 and the Zr rich corner is identical to that proposed by Nieva and Arias [6] at 800 °C. Two intermediate compounds were observed at 800 °C between Fe_2Zr(*C*15) and the pure Zr: $FeZr_3$ and $FeZr_2$. While at 900 °C, only $FeZr_2$ compound was observed [6,7].

According to the aims of this work, described in the Introduction section, a discussion can be based on the comparison of the present section with that obtained at 900 °C by Savidan et *al.* [7] in the region under study. The stable phases observed at 900 °C are also observed at 800 °C (only X″ was not observed because no alloy was synthesized in this region). This includes the presence of the *C*36 phase, probably stabilized from the high-temperature binary phase in Fe-Zr system [13] by Sn substitution in a process similar to that observed in Al-Co-Nb system [16]. The two-phase equilibria and tie-triangles are the same as at 900 °C so that it can be concluded that no ternary invariant reaction exist between the two temperatures. This is an important information for a future Calphad modelling of this system.

More quantitatively, Fig. 8 presents a comparison of the raw results of Savidan et *al.* [7] at 900 °C and from the present work at 800 °C. A comparison of the positions of the tie-triangles measured in both case can be done. Some of them conserved at 800 °C the position they had at 900 °C ([Fe_6Sn_6Zr- Sn(liq)-N], [Y-Fe_6Sn_6Zr-N]). A new tie-triangle anticipated in the work by Savidan et *al.* [7] was shown and measured in the present work ([Fe_2Zr(*C*15)-N-X′]). It stands at a significantly different position as testified by the presence of a tie-line N-Fe_2Zr(*C*15) (alloy 14 in the work by Savidan et

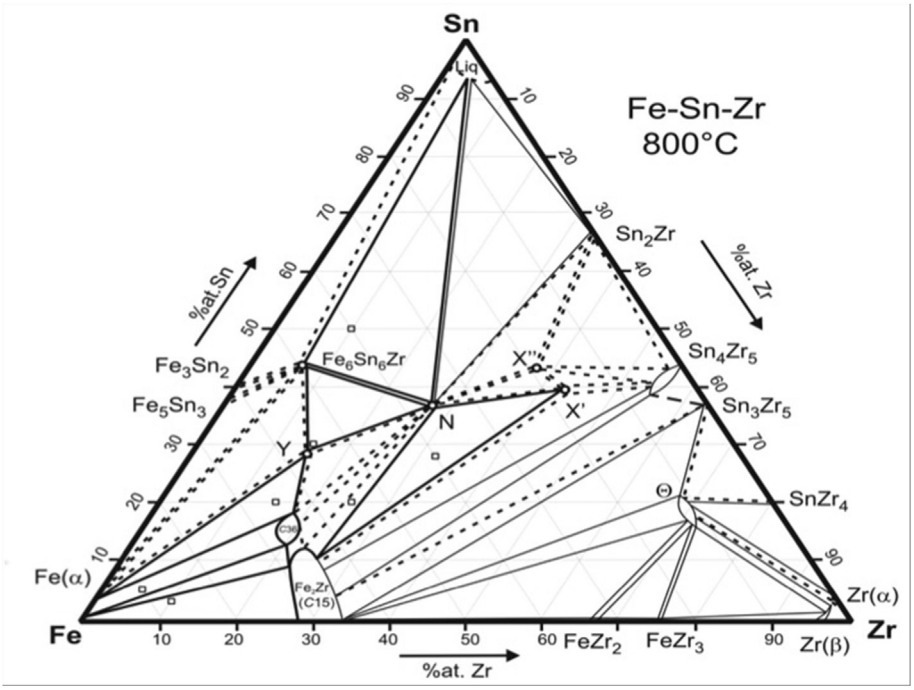

Fig. 7. Phase diagram of Fe-Sn-Zr proposed at 800 °C. (□) Nominal alloy compositions. Limits of phases: (—) thin lines measured by Nieva and Arias [6], thick lines measured in the present work, (—) probable.

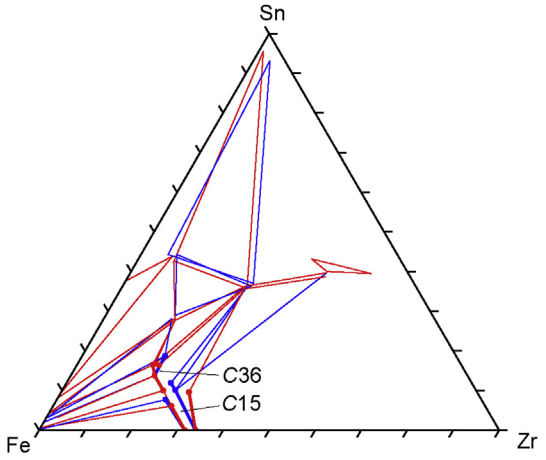

Fig. 8. Comparison of the micro-analysis results (tie-lines and tie-triangles) obtained by Savidan et *al.* [7] at 900 °C (in red) and in the present work at 800 °C (in blue). The limits of the homogeneity domains of Fe_2Zr(*C*15) and *C*36 phases are emphasized with thicker lines. (For interpretation of the references to colour in this figure legend, the reader is referred to the web version of this article.)

al.), covered in the present work by the tie-triangle [Fe_2Zr(*C*15)-N-X′]. This results in a homogeneity domain for the Fe_2Zr(*C*15) phase at 800 °C extending parallel to Sn-Zr border contrary to what is observed at 900 °C. Finally, the *C*36 corner of the tie-triangle [Fe(α)-Y-*C*36], observed in the two studies has a significantly different composition. This implies a homogeneity domain of the *C*36 phase that has not shrunk compared to 900 °C but has been displaced toward Sn-richer composition.

These differences but also, as importantly, the similarities between the isothermal sections at 800 °C and 900 °C will allow, to some extent, to assess the temperature dependent ternary parameters in the planned thermodynamic assessment of this system.

5. Conclusions

Using alloys equilibrated after long annealing times and the preliminary results published in previous work [6], an isothermal section at 800 °C of the system Fe-Sn-Zr has been constructed. This isothermal section advantageously complete that at 900 °C determined previously [7] yielding the possibility of a sound future thermodynamic description of the system by the Calphad method, allowing more reliable extrapolations at the low temperatures at which these alloys are used in the nuclear industry.

Acknowledgements

This work was supported by the Research Council of the National University of Tucumán (CIUNT) through Project and 26/E433 and a Grant CIUNT. We thank to E. Gonzo and P. Villagrán (LASEM-UN Salta), Nora Loureiro (Ezeiza Atomic Center, CNEA), and Gustavo Castellano and Marcos Oliva (LAMARX, FaMAF, UN Córdoba).

References

[1] L.E. Tanner, D.W. Levinson, The system Zr-Fe-Sn, Trans. ASM 52 (1960) 1115–1136.
[2] D.L. Kudryatsev, I.A. Tregubov, The Zr corner of the phase diagram and properties of alloys in the Zr-Fe-Sn system, Fiz.-Khim. SplavovTsirkoniya 133 (1968).
[3] N.V. Korotkova, The zirconium corner of the phase diagram Zr-Sn-Fe, Russ. Metall. 5 (1990) 201–208.
[4] N. Nieva, D. Arias, A new ternary compound in the Zr-Sn-Fe system, J. Nucl. Mater 277 (1) (2000) 120–122.
[5] N. Nieva, D. Arias, Experimental Phase Diagram of the Central Region of the Zr-Sn-Fe System, presented at CALPHAD XXX, York, England, 2001.
[6] N. Nieva, D. Arias, Experimental partial phase diagram of the Zr-Sn-Fe system, J. Nucl. Mater. 359 (1) (2006) 29–40.
[7] J.-C. Savidan, J.-M. Joubert, C. Toffolon-Masclet, An experimental study of the Fe-Sn-Zr ternary system at 900 °C, Intermetallics 18 (11) (2010) 2224–2228.
[8] Y.-U. Kwon, S.C. Sevov, J.D. Corbett, Substituted W5Si3- and Zr6Al2Co type phase formed in the zirconium-antimony and zirconium-tin systems with iron group metals, Chem. Matter 2 (5) (1990) 550–556.
[9] V. Raghavan, The Fe-Sn-Zr (Iron-tin-zirconium) System in Phase Diagrams of

Ternary Iron Alloys, 6B, Indian Inst. Metals, Calcutta, 1992, pp. 1199–1204.
[10] C.A. Alexander, J.S. Ogden, Thermodynamic activities in Zircaloy-4 by mass-spectrometry, J. Nucl. Mater 175 (3) (1990) 197–202.
[11] S. Liu, Y. Du, H. Xu, B. Huang, in: Günter Effenberg, Svitlanallyenko (Eds.), Iron-Tin-zirconium in Iron Systems: Phase Diagrams, Crystallographic and Thermodynamic Data, Part of Landolt-Börnstein - Group IV Physical Chemistry, Iron Systems, Part 5, Springer, 2009, pp. 1–19.
[12] T. Mazet, B. Malaman, Local chemical and magnetic disorder within the HfFe6Ge6-type RFe6Sn6 compounds (R=Sc, Tm, Lu and Zr), J. Magnetism Magnetic Mater. 219 (1) (2000) 33–40.
[13] F. Stein, G. Sauthoff, M. Palm, Experimental determination of intermetallic phases, phase equilibria, and invariant reaction temperatures in the Fe-Zr system, J. Phase Equilibria 23 (6) (2002) 480–494.
[14] N. Nieva, J. Jiménez, A. Gómez, D. Arias, M.S. Granovsky, Diagrama de fases experimental Zr-Fe y Zr-Sn-Fe de la zona rica en Fe a la temperatura de 1100 °C, Actas XI IBEROMET/CONAMET/SAM, 2010.
[15] G. Melnyk, A. Leithe-Jasper, P. Rogl, R. Skolozdra, The antimony-iron-zirconium (Sb-Fe-Zr) system, J. Phase Equilibria 20 (5) (1999) 497–507.
[16] O. Dovbenko, F. Stein, M. Palm, O. Prymak, Experimental determination of the ternary Co-Al-Nb phase diagram, Intermetallics 18 (11) (2010) 2191–2207.
[17] H. Okamoto, in: H. Okamoto (Ed.), Fe-Sn (Iron-Tin) in phase diagrams of binary iron alloys, ASM Int. Materials Park, 1993, pp. 385–392.